NASA/TM—2004-213206 AIAA–2004–3784

Computational Ion Optics Design Evaluations

Shane P. Malone and George C. Soulas
Glenn Research Center, Cleveland, Ohio

August 2004

The NASA STI Program Office . . . in Profile

Since its founding, NASA has been dedicated to the advancement of aeronautics and space science. The NASA Scientific and Technical Information (STI) Program Office plays a key part in helping NASA maintain this important role.

The NASA STI Program Office is operated by Langley Research Center, the Lead Center for NASA's scientific and technical information. The NASA STI Program Office provides access to the NASA STI Database, the largest collection of aeronautical and space science STI in the world. The Program Office is also NASA's institutional mechanism for disseminating the results of its research and development activities. These results are published by NASA in the NASA STI Report Series, which includes the following report types:

- TECHNICAL PUBLICATION. Reports of completed research or a major significant phase of research that present the results of NASA programs and include extensive data or theoretical analysis. Includes compilations of significant scientific and technical data and information deemed to be of continuing reference value. NASA's counterpart of peer-reviewed formal professional papers but has less stringent limitations on manuscript length and extent of graphic presentations.

- TECHNICAL MEMORANDUM. Scientific and technical findings that are preliminary or of specialized interest, e.g., quick release reports, working papers, and bibliographies that contain minimal annotation. Does not contain extensive analysis.

- CONTRACTOR REPORT. Scientific and technical findings by NASA-sponsored contractors and grantees.

- CONFERENCE PUBLICATION. Collected papers from scientific and technical conferences, symposia, seminars, or other meetings sponsored or cosponsored by NASA.

- SPECIAL PUBLICATION. Scientific, technical, or historical information from NASA programs, projects, and missions, often concerned with subjects having substantial public interest.

- TECHNICAL TRANSLATION. English-language translations of foreign scientific and technical material pertinent to NASA's mission.

Specialized services that complement the STI Program Office's diverse offerings include creating custom thesauri, building customized databases, organizing and publishing research results . . . even providing videos.

For more information about the NASA STI Program Office, see the following:

- Access the NASA STI Program Home Page at ***http://www.sti.nasa.gov***

- E-mail your question via the Internet to help@sti.nasa.gov

- Fax your question to the NASA Access Help Desk at 301–621–0134

- Telephone the NASA Access Help Desk at 301–621–0390

- Write to:
  NASA Access Help Desk
  NASA Center for AeroSpace Information
  7121 Standard Drive
  Hanover, MD 21076

NASA/TM—2004-213206 AIAA–2004–3784

Computational Ion Optics Design Evaluations

Shane P. Malone and George C. Soulas
Glenn Research Center, Cleveland, Ohio

Prepared for the
40th Joint Propulsion Conference and Exhibit
cosponsored by AIAA, ASME, SAE, and ASEE
Fort Lauderdale, Florida, July 11–14, 2004

National Aeronautics and
Space Administration

Glenn Research Center

August 2004

This report contains preliminary findings, subject to revision as analysis proceeds.

Available from

NASA Center for Aerospace Information
7121 Standard Drive
Hanover, MD 21076

National Technical Information Service
5285 Port Royal Road
Springfield, VA 22100

Available electronically at http://gltrs.grc.nasa.gov

Computational Ion Optics Design Evaluations

Shane P. Malone and George C. Soulas
National Aeronautics and Space Administration
Glenn Research Center
Cleveland, Ohio 44135

Ion optics computational models are invaluable tools in the design of ion optics systems. In this study a new computational model developed by an outside vendor for use at the NASA Glenn Research Center (GRC) is presented. This computational model is a gun code that has been modified to model the plasma sheaths both upstream and downstream of the ion optics. The model handles multiple species (e.g. singly and doubly-charged ions) and includes a charge-exchange model to support erosion estimations. The model uses commercially developed solid design and meshing software to allow high flexibility in ion optics geometric configurations. The results from this computational model are applied to the NEXT project to investigate the effects of crossover impingement erosion seen during the 2000-hour wear test.

Nomenclature

A	=	constant	t	=	time
B	=	constant	T_e	=	electron temperature, eV
d_a	=	accelerator grid aperture diameter	T_{ed}	=	downstream electron temperature, eV
d_s	=	screen grid aperture diameter	T_{eu}	=	upstream electron temperature, eV
e	=	elementary charge, 1.619×10^{-19} C	v_b	=	beam ion velocity, m/s
E_b	=	beam fast particle energy, eV	v_{id}	=	downstream ion velocity, m/s
j_i	=	ion current density, A/m^2	V_a	=	accelerator grid voltage, V
$j_{beamlet}$	=	ion beamlet current density, A/m^2	V_{net}	=	net accelerating voltage, V
J_b	=	ion beam current, A	V_s	=	screen grid voltage, V
m_{Xe}	=	xenon atom or ion mass, 2.193×10^{-25} kg	Xe	=	neutral xenon atom
n_b	=	beam fast particle density, m^{-3}	Xe^+	=	singly-charged xenon ion
n_e	=	electron number density, m^{-3}	Xe^{++}	=	doubly-charged xenon ion
n_i	=	ion number density, m^{-3}	ϕ	=	local plasma potential, V
n_{id}	=	downstream ion number density, m^{-3}	ϕ_u	=	upstream plasma potential, V
n_{iu}	=	upstream ion number density, m^{-3}	ϕ_d	=	downstream plasma potential, V
n_n	=	neutral number density, m^{-3}	ϕ_p	=	bulk plasma potential, V
r	=	ion optics radial distance, mm	σ_{cex}	=	charge exchange cross section, Å^2

I. Introduction

Ion optics computational models are invaluable tools in the development of new ion engine optics and in the assessment of current ion optics designs. Ion optics models can be used as design tools to determine the best optics aperture size and grid spacing by assessing optics performance. A good ion optics model should be capable of predicting perveance of the optics, both direct and crossover impingement limits, beam divergence, and electron backstreaming limits. Ideally, the model should run relatively quickly and without the use of expensive mainframe computers. This allows the user to assess multiple iterations of a design in a short period of time.

Ion optics models are also useful in assessing the service life and wearout mechanisms of a set of ion optics. By calculating the impingement of beam ions and charge exchange ions on the accelerator grid, ion optics models should be able to predict the erosion of ion optics over life. Performance modeling at different times in life with new wearout geometries can be used to assess the effects of erosion on perveance, beam divergence, and electron backstreaming.

Current and future ion thruster development programs will make extensive use of ion optics computational models to reduce design time and ion optics design iterations. This will allow optics to be designed and produced more effectively and quickly, at a lower cost to the development program. The NASA Evolutionary Xenon Thruster (NEXT) program has made use of ion optics models to determine the service life assessment of the ion optics,[1,2] and optics modeling was instrumental in the selection of Thick Accelerator Grid (TAG) optics geometry over the state-of-the-art NASA Solar electric propulsion Technology Applications Readiness (NSTAR) thruster ion optics geometry for the NEXT program. Additional ongoing work at NASA GRC in the development of high specific impulse, long life ion optics makes extensive use of ion optics modeling.[3] Other future thruster developments will likely require new ion optics designs and will also make extensive use of ion optics models to develop them.

There are many ion optics models which have been developed in the last twenty years, some of which are described below. This is by no means a complete list of optics models, but is meant to illustrate the variety of approaches to the problem of ion optics modeling in the past and present.

Ion optics models are most easily sorted into two-dimensional (2D) and three-dimensional (3D) models. Two-dimensional optics models are generally much faster to run than 3D models, owing to their relative simplicity and assumption of axisymmetry. Two-dimensional models have been developed and used at the University of Michigan,[2] University of Tokyo,[4] and the Keldysh Research Center.[5] Unfortunately, the assumption of axisymmetry which allows the 2D models to be run much faster than 3D models introduces some inherent limitations in their capabilities, namely that they cannot predict over-focusing well, and that they cannot determine impingement patterns on downstream surface of the accelerator grid in a two-grid optics system. However, for situations where barrel erosion is the dominant wearout mechanism, such as three-grid optics systems and some two-grid optics systems, 2D codes have applications in service life assessment.

Three-dimensional optics models are generally more useful than 2D models for optics design and service life assessment, with the drawback that many models cannot be run quickly on personal computers without some simplifying assumptions. This limits the amount of design iterations that can be evaluated. Three-dimensional models have been developed by University of Tennessee Space Institute,[6] Colorado State University,[7] University of Tokyo,[8] and jointly by the Virginia Polytechnic Institute and the Jet Propulsion Laboratory.[9]

In this paper, a commercially developed, fully three-dimensional ion optics computational model with tremendous flexibility is presented. This model uses commercial, off-the-shelf computer aided design software and a similarly available commercial meshing package as the front end, allowing modeling of single and multiple apertures, varied aperture shapes and grid spacing, and the commonly seen cusp geometry along grid aperture barrels, as well as misaligned apertures. This geometric flexibility allows investigations of new geometrical concepts. The model is also capable of modeling multiple charge state ions and multiple generations of charge exchange (CEX) ions and neutrals. Through the use of reflective boundary conditions, the model can simulate adjacent apertures rather than modeling them directly, and can also simulate the effects of edge apertures and "missing" holes along the edge where the hole pattern ends. This optics model is currently being used to evaluate the TAG optics on the NEXT thruster. Preliminary results from this evaluation are presented.

II. Ion Optics Computational Model Description

The ion optics computational model developed for NASA GRC is a new three-dimensional electrostatic equilibrium particle-in-cell (PIC) code that has been designed to address the recent beam optics modeling and simulation requirements for vacuum electron devices, ion sources, and charged-particle transport. The model combines modern finite-element techniques with improved physics models. The code employs a conformal mesh, including both structured and unstructured mesh architectures for meshing flexibility, along with a new method for accurate, efficient particle tracking. New particle emission/creation models include space-charge-limited emission, charge exchange, thermionic beam representation, and secondary electron emission. One of the key features of the code is its ability to model fine-scale features in a large volume. This makes it valuable for performing sensitivity studies and generating manufacturing tolerance specifications.

Although the code is still in development, it has been specifically designed to model ion thruster optics. Currently, much emphasis is being placed on validating the code against experimental data and other models. This is especially necessary for ion thruster modeling, where detailed knowledge of the physical parameters is difficult to ascertain.

For ion thruster modeling, the need for three-dimensional simulation of volumetric ion sources, ion acceleration, and optics geometry, with the ability to model charge exchange of the ion beam with a background neutral gas are important features to be captured. The two pieces of physics that stand out as significant are modeling of the upstream and downstream plasma sources and modeling of charge exchange.

The numerical solution employed by the code combines finite element analysis with particle-in-cell (PIC) methods. The basic physics model is based on the equilibrium steady-state application of the electrostatic particle-in-cell (PIC) approximation employing a conformal computational mesh. The foundation of the model stems from the same basic electron gun code model introduced in codes such as EGUN.[10] Here, Poisson's equation is used to self-consistently include the effects of space charge on the fields, and the relativistic Lorentz equation is used to integrate the particle trajectories through those fields.

Gun models have been around since the 1970s, and have been a mainstay in the vacuum electronics and accelerator communities for beam formation modeling. As shown in Figure 1, in the gun model the fields are held frozen while the particles are tracked through the system. As the particles are tracked, they lay down charge on the mesh, which is subsequently used to update the fields. This series of steps is repeated until the beam tracking and fields stop evolving, and results in the self-consistent steady-state equilibrium condition. The benefit of this method over time-domain models is that there are no time-related transients that have to be flushed out of the simulation, and the expensive field solution step is not done every step. These simulations can be orders of magnitude faster than time-domain solutions.

For ion thruster modeling, several modifications and additions to the basic electron gun code model needed to be made, including:

- inclusion of ions and neutrals,
- a model to support the ion plasma source, and
- addition of a charge exchange model.

These new features were not trivial to add to the gun model, but fortunately the gun model supports the architecture needed for their implementation.

In the new code, the method for modeling the plasma sheath that forms in ion sources assumes that the electron distribution function is a Maxwellian function of electrostatic potential over electron temperature. The plasma model feature supports the development of a sheath in both the upstream ion source and downstream plasma. Separate upstream and downstream models are included that supports thruster modeling. The electrons are included numerically as Boltzmann electrons with a density calculated per Equation 1.

$$n_e = n_i e^{\frac{\phi - \phi_p}{T_e}} \tag{1}$$

The source faces of the mesh can support multiple species per source face so that Xe^+ and Xe^{++} can be injected simultaneously. The model is not constrained by imposing a Dirichlet boundary condition that dictates the potential at the plasma boundaries. As a result this potential is calculated self-consistently. However, the user can impose a Dirichlet boundary condition if desired.

Charge exchange is the process by which a "fast" charged particle streaming through a neutral background gas collects an electron from a "slow" neutral particle, resulting in a fast neutral and a slow charged particle. An efficient method for capturing this is essential. The model supports multiple charge exchange reactions, including the following:

$$Xe^{+}_{fast} + Xe_{slow} \rightarrow Xe_{fast} + Xe^{+}_{slow}$$
$$Xe^{++}_{fast} + Xe_{slow} \rightarrow Xe_{fast} + Xe^{++}_{slow}$$
$$Xe^{++}_{fast} + Xe_{slow} \rightarrow Xe^{+}_{fast} + Xe^{+}_{slow}$$

The charge exchange collision rate follows Equation 2. A semi-empirical model by Miller, et al[11] was used for the charge exchange algorithm, shown in Equation 3. The CEX algorithm implemented handles multiple generations of charge exchange. The self-consistent space charge is included in the Poisson solution, so that the effects of source and CEX products are captured. The subsequent fast neutral particles are tracked for possible collisions with the grids. The model currently performs one "reaction" per cell, where the source particles are binned and multiple launches can be made per "reaction". Here, the source ions are velocity-binned (bins chosen by user), and each launch creates one launch pair per bin. This allows the code to capture the effect of a distribution, while allowing the total particle count to stay in check.

$$\frac{dn_b}{dt} = -n_b n_n v_b \sigma_{cex} \tag{2}$$

$$\sigma_{cex} = A - B \log(E_b) \tag{3}$$

III. Model Application to NEXT

A. Problem

During the NEXT 2000-hour wear test, accelerator apertures in the outer 47 mm of the grids exhibited an off-center, hexagonal star-shaped erosion pattern.[12] The eroded points of the stars were chamfered through the electrode thickness and extent of the erosion pattern generally increased with increasing ion optics' radius (see Figure 2). It was determined that this erosion likely occurred early in the wear test and at lower beam current operation (1.20 A and 2.70 A). Erosion was most likely due to a combination of effects, including:

1. over-focusing of beamlet ions due to low plasma density near the grid edges;
2. significantly smaller-than-nominal accelerator aperture diameters in this region; and
3. misaligned screen and accelerator apertures due to an under-compensated hole pattern.

Over-focusing of ion beamlets generally occurs in areas where there is low plasma density, such as near the edge apertures and when the thruster is operated at a lower beam current. The normalized perveance per hole drops to values much less than one, and the plasma sheath migrates further upstream. This highly distorted sheath tends to draw ions across the beam centerline, where, in extreme cases, they impinge on the accelerator grid aperture barrel. This effect is generally referred to as crossover impingement.

Due to manufacturing difficulties associated with etching the TAG optics on the NEXT engine, hole sizes near the edge were more than 10% smaller than the nominal hole size. Figure 3 and Figure 4 show the accelerator and screen grid aperture sizes as a function of radius. Smaller holes in the accelerator grid mean that it is easier for over-focused ions to strike the barrel of the aperture.

Under-compensation of the hole pattern means that the screen and accelerator grid apertures are not co-linear but are misaligned such that the outer beamlets are deflected away from the thrust axis. A misaligned set of apertures would be more susceptible to grid erosion due to electric fields which pull the ion beamlet away from the geometric centerline of the holes.

B. Optics Model Assessment

The ion optics computational model is being used to assess the over-focusing of the beamlets in the low density regions of the NEXT ion optics. Preliminary evaluation of over-focusing is being performed for engine operation at 3.52 A beam current and 1.20 A beam current, at radial locations of 153 mm (where erosion patterns were first noticed) and 199 mm (the last edge aperture). Current density values and aperture sizes are directly from measurements taken during the NEXT 2000-hour wear test and subsequent examination. Aperture sizes were determined by averaging the positive and negative aperture sizes shown in Figure 3 at each radial location. Thruster current density profiles for 3.52 A and 1.20 A cases are shown in Figure 5. A nominal grid was used in these calculations. Model inputs are shown in Table 1.

Screen and accelerator voltages were those used during the 2000-hour test. Plasma parameters were determined based on plasma diagnostics during the test. Upstream plasma density was determined by assuming that the upstream plasma ion current was the Bohm current, and calculated from Equation 4.

$$n_i = \frac{j_i}{e}\sqrt{\frac{m_{Xe}}{T_e}} \tag{4}$$

The downstream plasma density was estimated using Equation 5, where ion velocity downstream is determined from conservation of energy, Equation 6.

$$n_{id} = \frac{j_{beamlet}}{e v_{id}} \tag{5}$$

$$v_{id} = \sqrt{\frac{2eV_{net}}{m_{Xe}}} \tag{6}$$

The effects of CEX ions and neutrals were not considered for this initial analysis, but will be investigated at a later time.

C. Geometric Configurations

Several model mesh geometries were used to attempt to determine the effects of over-focusing and crossover impingement. These included co-linear screen and accelerator grid apertures using both smooth barrels and the cusp geometry shown in Figure 6, as well as apertures which were misaligned by up to 4% of the nominal screen grid aperture diameter, as shown in Figure 7.

In most cases, a hexagonal, reflective boundary condition (see Figure 8) was used to determine the proper ion impingement patterns on the accelerator grid aperture barrel, but a cylindrical boundary condition was used for cusp cases because the model was easier to create. Incorporation of the cusp geometry with the hexagonal reflective boundary condition will be implemented in the future.

Because areas of the ion thruster with low plasma density and low ion current density are being investigated, a long upstream area is required in order to allow the upstream plasma potential to reach equilibrium and the sheath to form properly. The upstream area length is 3.2 times longer than the nominal screen grid aperture diameter. This provides adequate upstream distance for the extended sheath and pre-sheath to set up and reach equilibrium at the plasma potential. In order to reduce computational time, mesh elements at the upstream boundary to the model are quite long, but get smaller as they approach the screen grid. This allows the model to focus more on the strong electric field region of the optics. The downstream area is similarly configured, with mesh elements growing longer as they get further from the downstream surface of the accelerator grid. An example of the mesh is shown in Figure 9.

There are 1947 source faces at the upstream mesh boundary. From each source face, 3 emission macroparticles are injected. Each macroparticle represents a number of ions such that the total current density required for the case is maintained.

D. Preliminary Results

Figure 10 and Figure 11 show the equipotential lines and ion trajectories for the r = 199 mm cases. Normalized perveance per hole was calculated per Reference 3, giving values of 0.006 and 0.021 for the J_b = 1.20 A and 3.52 A cases, respectively. The J_b = 1.20 A case shows clear evidence of crossover impingement along the accelerator grid aperture barrel by over-focused beam ions. However, the J_b = 3.52 A case shows that there is either no impingement or very little impingement, a result that is surprising given the extent of the erosion shown in Figure 2. Further refinement of the model geometry and input parameters will be necessary to determine whether crossover impingement does actually occur for this operating condition.

For the J_b = 1.20 A case, impingement current density was plotted on the 3D surface of the accelerator aperture barrel to determine the qualitative erosion pattern (see Figure 12). A future improvement in the model will include the ability to show impingement current for ions of different energies in order to calculate the erosion rate directly. The most current is deposited near the downstream surface of the accelerator aperture barrel, and in six directions indicating the points of the hexagonal boundary. The points of the hexagonal boundary correspond to the webbing directions as shown in Figure 8. As shown in Figure 2, for apertures which are fully surrounded by holes (r = 184 and 195 mm pictures), there is preferential erosion along the webbing direction. This is most likely due to upstream sheath distortion caused by the proximity of adjacent holes. Figure 2 shows that at r = 199 mm, where the hole pattern ends, a different erosion pattern emerges, most likely due to the "missing" holes beyond the hole pattern. This effect will be investigated further in the future.

Figure 13 and Figure 14 show the equipotential lines and ion trajectories for the r = 153 mm cases. Normalized perveance per hole was calculated per Reference 3, giving values of 0.055 and 0.161 for the J_b = 1.20 A and 3.52 A cases, respectively. Neither the J_b = 1.20 A nor the J_b = 3.52 A cases show any evidence of crossover impingement. This most likely indicates that the erosion seen in the NEXT 2000-hour test at this aperture locations was not caused primarily by the low upstream plasma density as in the r = 199 mm case. To investigate other geometric reasons for the erosion, the effects of cusps and misaligned apertures were investigated. The model was run for these geometries using the same conditions shown in Table 1 for the J_b = 1.20 A case.

Figure 15 and Figure 16 show the equipotential lines and particle trajectories for the cusp and misaligned aperture cases, respectively. There is still no evidence of impingement current on the accelerator aperture barrel for the cusp geometry. However, the electric field lines are distorted differently due to the change in geometry, an effect which could cause changes in the ion trajectory. Future calculations will combine the hexagonal boundary with the cusped aperture to provide the most realistic look at the optics geometry.

The misaligned apertures create electric fields which tend to slew the ion trajectories away from the direction of misalignment (in the case of the NEXT 2000-hour test, away from the thrust axis). This, combined with the low upstream plasma density, creates an over-focused beam which impacts the aperture barrel preferentially as shown in Figure 16. This preferential impingement is likely the cause of the slight erosion shown in Figure 2 for the r = 153 mm case.

IV. Future work

The ion optics computational model being developed for NASA-GRC will be used in the design of ion optics for future ion thrusters. Further investigation of the NEXT 2000-hour wear test results will include:

- Incorporation of the cusp geometry with the hexagonal boundary condition
- Investigation of varied grid gap dimension on crossover impingement
- Modeling of edge apertures to simulate "missing" apertures at the edge of the hole pattern
- Sensitivity analysis of input parameters such as T_{eup} and ϕ_{up} on crossover impingement
- Inclusion of CEX effects, including pit-and-groove erosion analysis
- Incorporation of ion energy with impingement current density to determine erosion

In order to more fully validate the results of the ion optics model, it will be compared to the results of the NSTAR LDT and ELT, as well as further data from the NEXT 2000-hour wear test. The model will also be compared to the results of other established computational models to validate certain characteristics.

V. Conclusions

The ion optics computational model being developed for NASA-GRC shows great flexibility in geometry due to its use of commercial computer aided design and meshing software as the front end. The code itself is capable of running on a personal computer, with detailed runs taking only a few hours to finish. The model was used to investigate crossover impingement erosion seen in the NEXT 2000-hour wear test. Preliminary comparison of model results to the wear test results demonstrate the model's flexibility in modeling various aperture geometries, but indicate that improvements to the model and to understanding of the input conditions must be made to fully predict over-focusing and crossover impingement. Further improvements in the model will enhance this capability.

References

[1] Farnell, C.C., Williams, J.D., and Wilbur, P.J., "NEXT Ion Optics Simulation via ffx," AIAA Paper 2003–4869, July 2003.

[2] Emhoff, J.W. and Boyd, I.D., "Grid Erosion Modeling of the NEXT Ion Thruster Optics," AIAA Paper 2003–4868, July 2003.

[3] Williams, G.J., Rawlin, V.K., and Soulas, G.C., "Long Life, High Specific Impulse Titanium Ion Optics," AIAA Paper 2003–4866, July 2003.

[4] Arakawa, Y. and Nakano, M., "Comparison of Two-Dimensional Optics Codes," AIAA Paper 1998–3801, July 1998.

[5] Muravlev, V.A., and Shagayda, A.A., "Numerical Modeling of Extraction Systems in Ion Thrusters," IEPC Paper 99–162, October 1999.

[6] Peng, X., and Keefer, D., "Plasma Particle Simulation of Electrostatic Ion Thrusters," *Journal of Propulsion and Power*, Vol 8. No. 2, 1992, pp. 361–366.

[7] Farnell, C.C., Williams, J.D., and Wilbur, P.J., "Numerical Simulation of Ion Thruster Optics," IEPC Paper 03–073, March 2003.

[8] Nakano, M. and Arakawa, Y., "Development of an Efficient Three-Dimensional Optics Code," IEPC Paper 97–015, August 1997.

[9] Wang, J. and Polk, J., "Three-Dimensional Particle Simulations of Ion Optics Plasma Flow and Grid Erosion," AIAA Paper 2002–2193, May 2002.

[10] Herrmannsfeldt, W.B., "EGUN—An Electron Optics and Gun Design Program," SLAC Report 331, Oct. 1988

[11] Miller, J.S., Pullins, S.H., Levandier, D.J., Chiu, Y., and Dressler, R.A., "Xenon charge exchange cross sections for electrostatic thruster models," *Journal of Applied Physics*, Vol 91. No. 3, 2002, pp. 984–991.

[12] Soulas, G.C. et al, "NEXT Ion Engine 2000-hour Wear Test Results", submitted for publication as AIAA Paper 2004–3791, July 2004.

Table 1. Model inputs for NEXT over-focusing.

	J_b = 1.20 A		J_b = 3.52 A	
	r = 153 mm	r = 199 mm	r = 153 mm	r = 199 mm
d_a	–6.7% from nominal	–15.6% from nominal	–6.7% from nominal	–15.6% from nominal
d_s	–2.7% from nominal	–2.7% from nominal	–2.7% from nominal	–2.7% from nominal
V_a	–260 V	–260 V	–220 V	–220 V
V_s	1765 V	1765 V	1766 V	1766 V
ϕ_u	1796 V	1796 V	1796 V	1796 V
ϕ_d	6 V	6 V	6 V	6 V
T_{eu}	6 eV	6 eV	6 eV	6 eV
T_{ed}	1 eV	1 eV	1 eV	1 eV
n_{iu}	3.30×10^{16} m^{-3}	3.38×10^{15} m^{-3}	9.89×10^{16} m^{-3}	1.29×10^{16} m^{-3}
n_{id}	1.37×10^{15} m^{-3}	1.41×10^{14} m^{-3}	4.12×10^{15} m^{-3}	5.37×10^{14} m^{-3}
$j_{beamlet}$	11.18 A/m^2	1.14 A/m^2	33.54 A/m^2	4.37 A/m^2

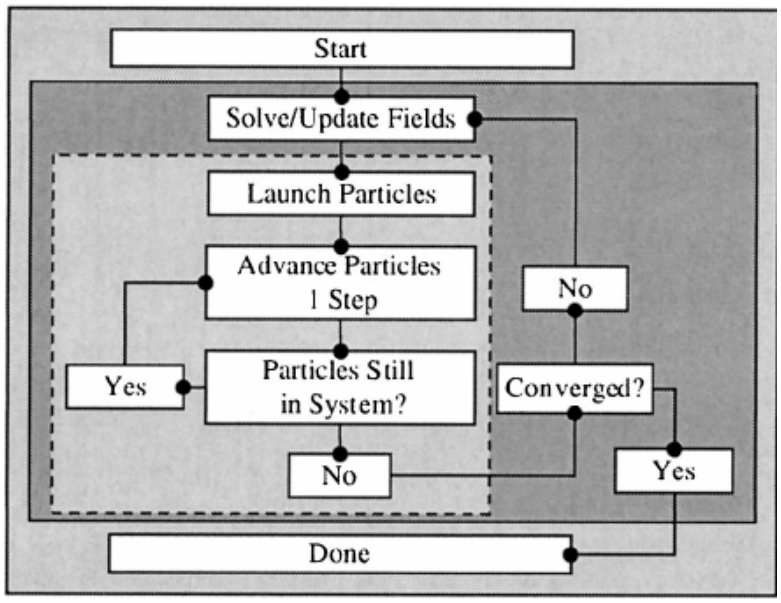

Figure 1. Basic gun code algorithm

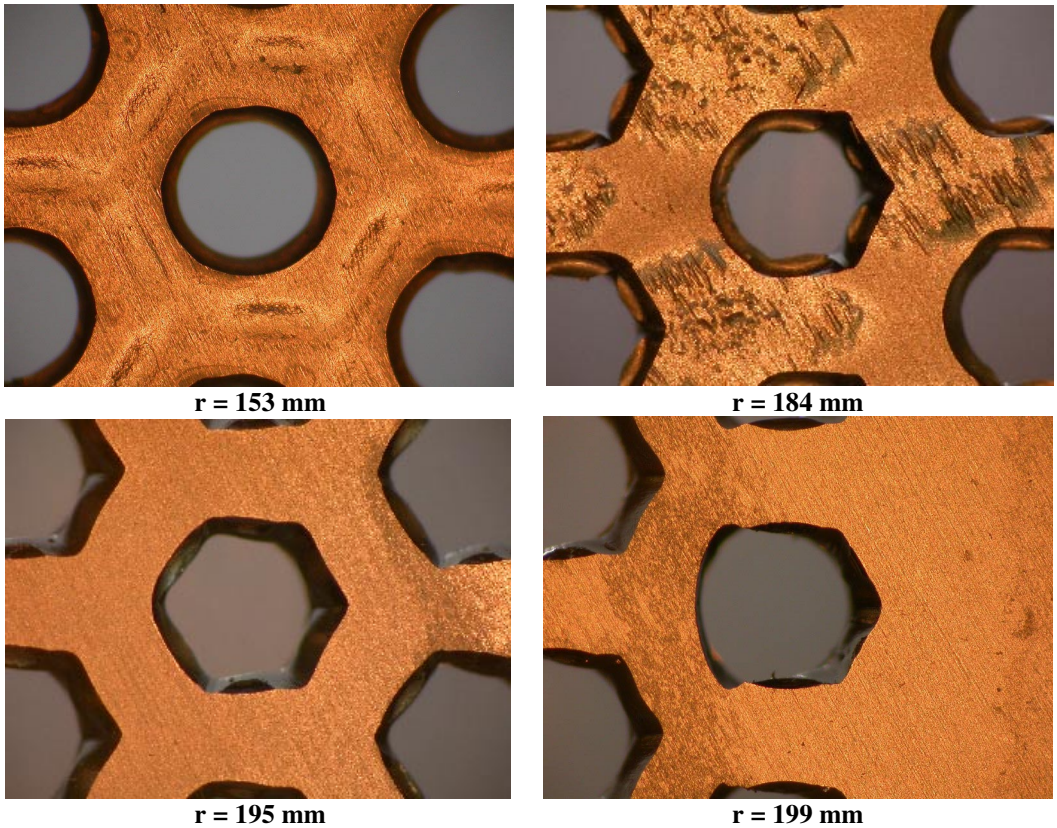

r = 153 mm **r = 184 mm**

r = 195 mm **r = 199 mm**

Figure 2. Post-test photomicrographs of NEXT downstream accelerator apertures at radial locations of 153, 184, 195 and 199 mm. Aperture erosion is less obvious at 153 mm but appears in the 4 o'clock area of the aperture. Aperture erosion at 184 and 195 mm shows preferential erosion along the webbing direction. Aperture erosion at 199 mm is distorted due to the absence of apertures to the right of the aperture shown.

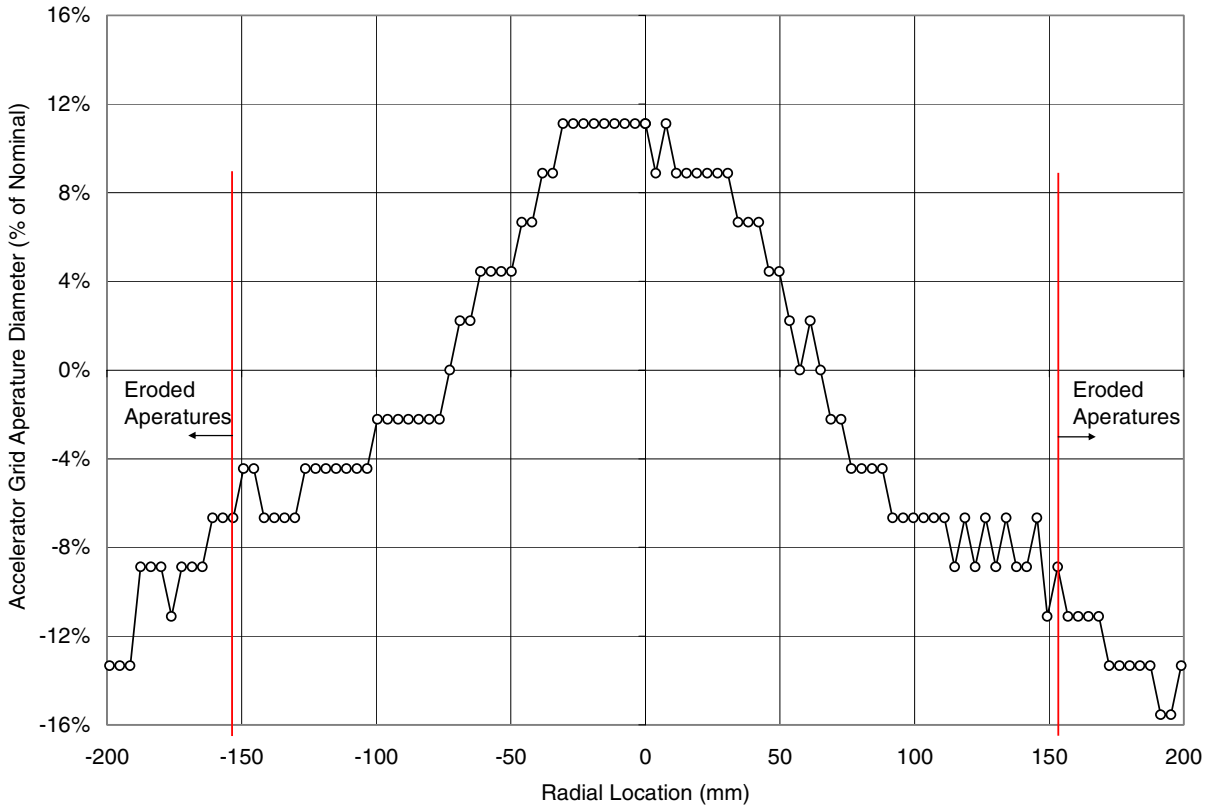

Figure 3. Pre-test accelerator aperture diameters as a function of radius. Diameters were measured with pin gages that were in increments of 2.2% of the nominal accelerator aperture diameter.

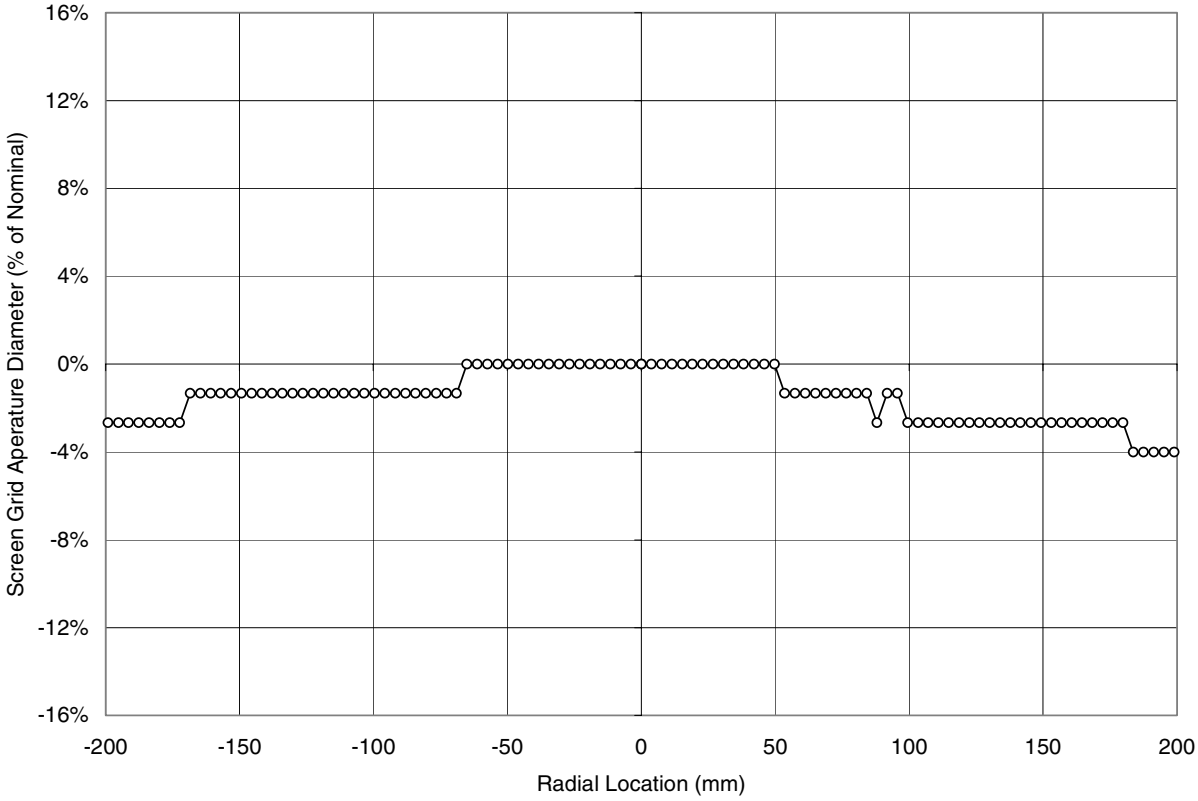

Figure 4. Pre-test screen aperture diameters as a function of radius. Diameters were measured with pin gages that were in increments of 1.3% of the nominal screen aperture diameter.

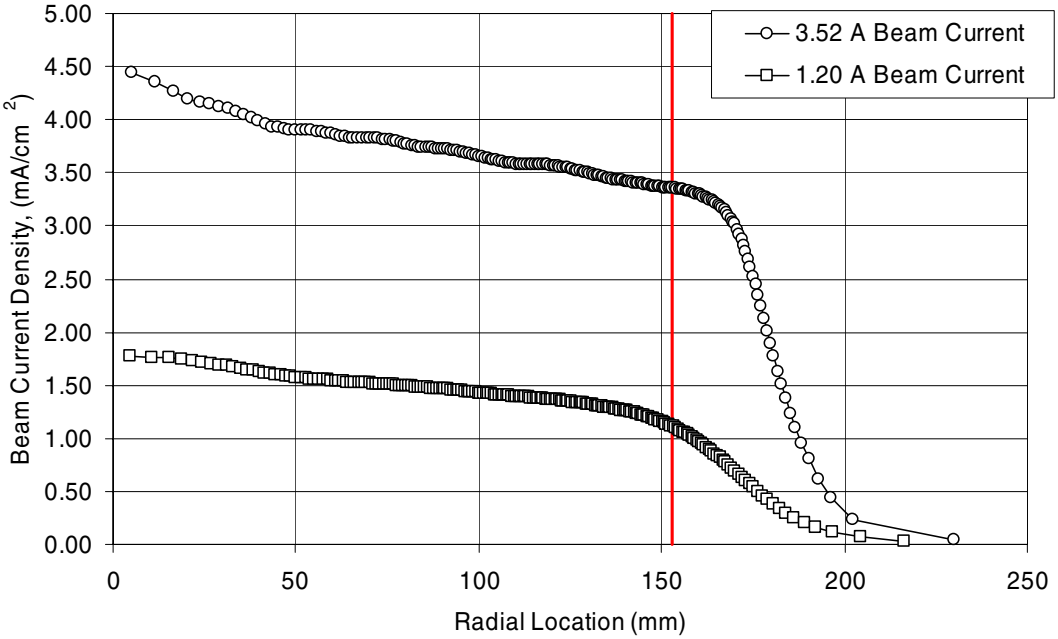

Figure 5. Beamlet current density as a function of radius for 1.20 A and 3.52 A beam current conditions. Line indicates location where aperture erosion begins.

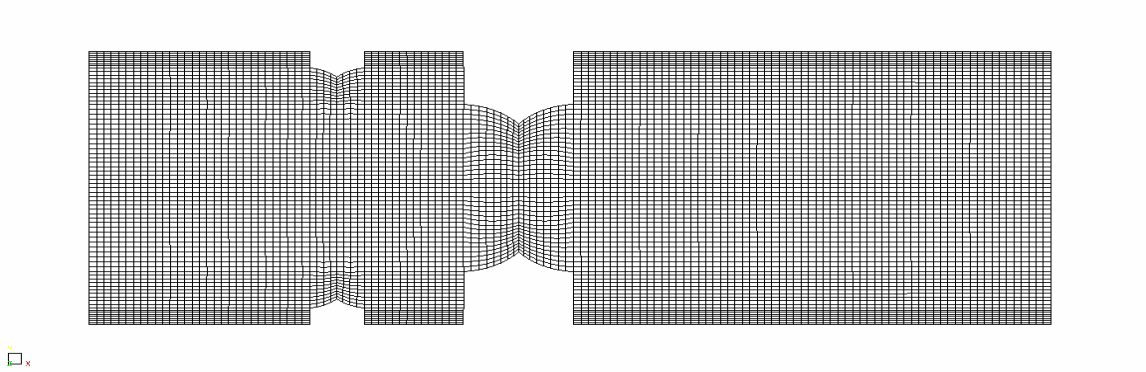

Figure 6. Aperture cusps were modeled. Aperture diameter at the cusp tips is the measured value in Figures 2 and 3. Cusp height is 20% of the nominal screen grid thickness and 33% of the nominal accelerator grid thickness.

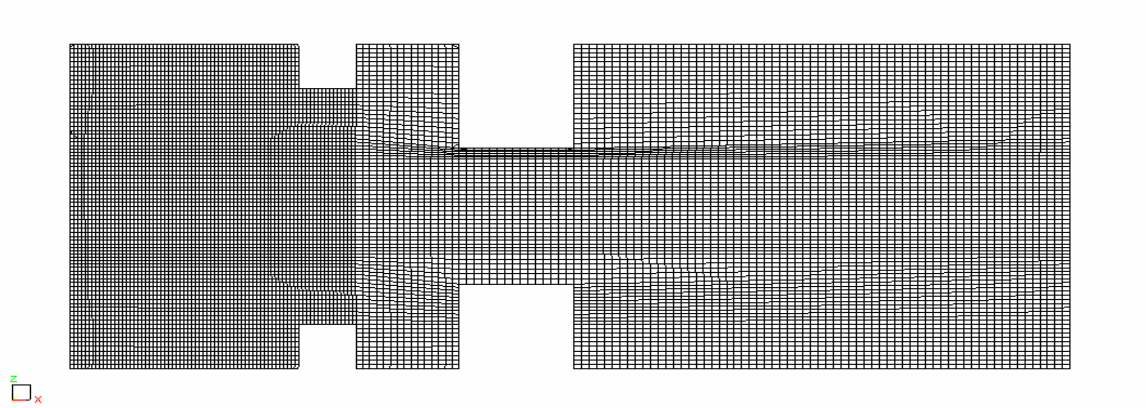

Figure 7. Misaligned apertures were modeled. Accelerator aperture centerline is offset from screen aperture centerline by 4% of nominal screen grid aperture diameter.

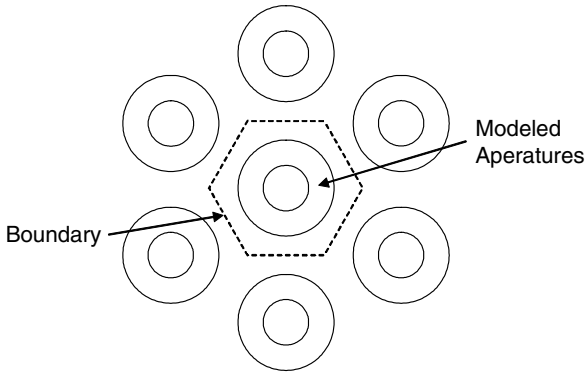

Figure 8. The ion optics model uses a full single aperture and a hex shaped reflective boundary to simulate adjacent apertures.

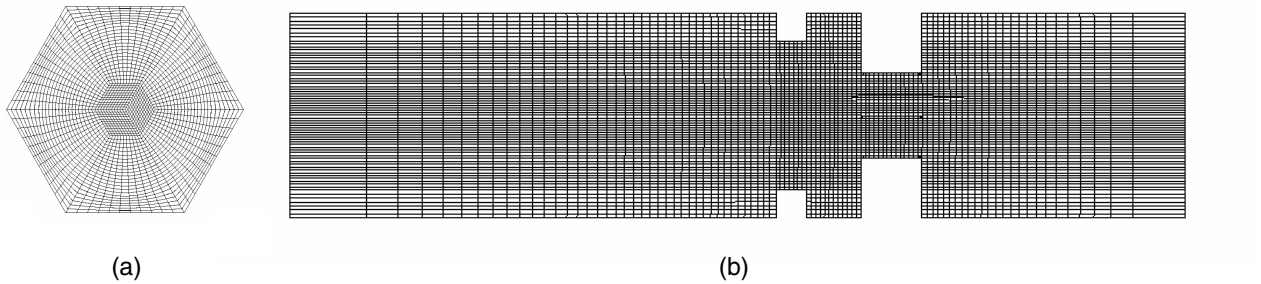

Figure 9. A cross-section of the hexagonal mesh geometry is shown in (a). A lengthwise cross-section of the mesh geometry is shown in (b).

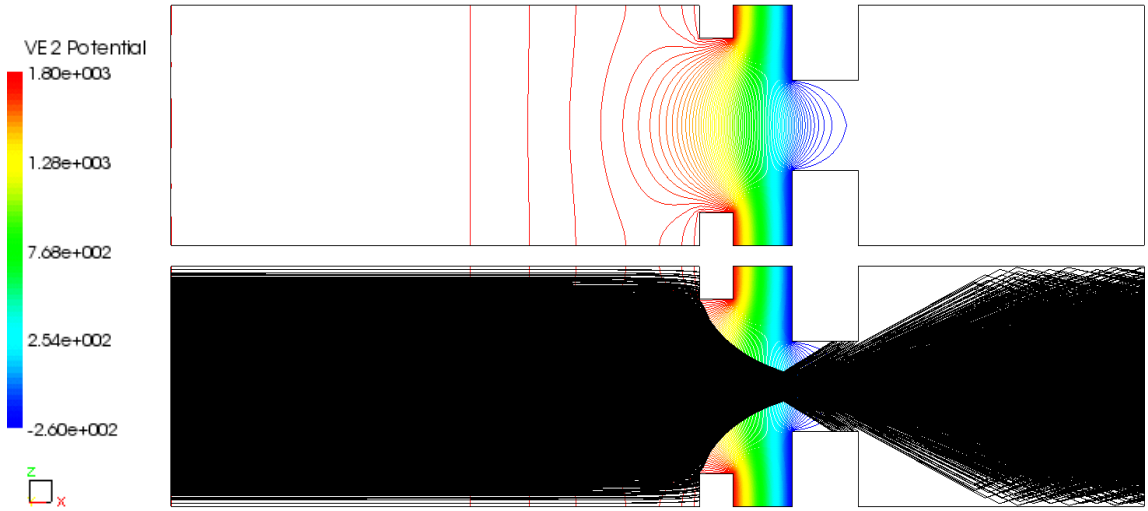

Figure 10. Equipotential lines and particle trajectories for r = 199 mm, J_b = 1.20 A case. The sheath is distorted well upstream of the screen grid, and crossover impingement is clearly indicated. Boundaries shown are from point to point on the hex boundary condition.

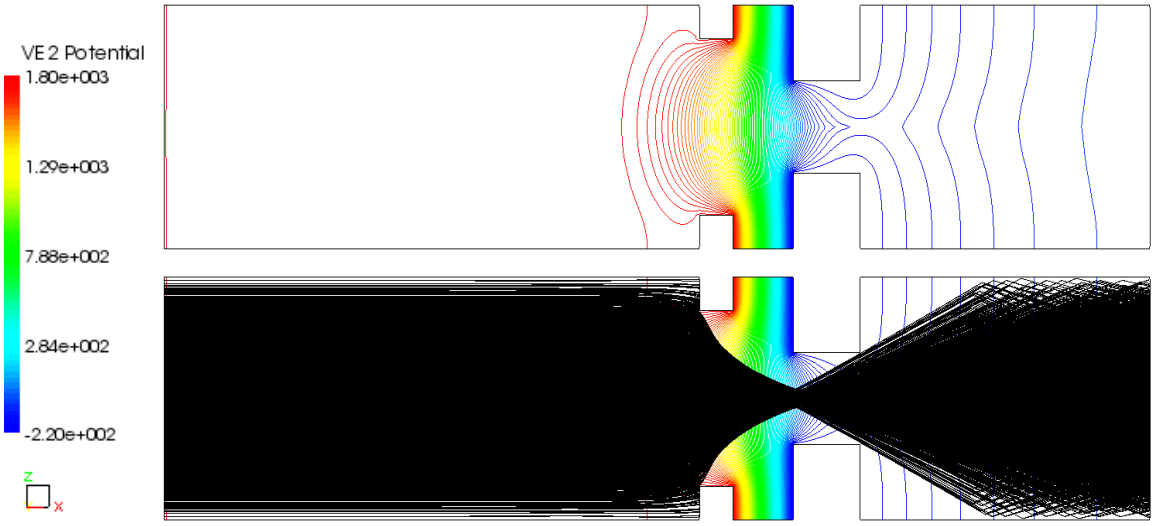

Figure 11. Equipotential lines and particle trajectories for r = 199 mm, J_b = 3.52 A case. The sheath is still distorted upstream of the screen grid, but crossover impingement is not clearly indicated. Boundaries shown are from point to point on the hex boundary condition.

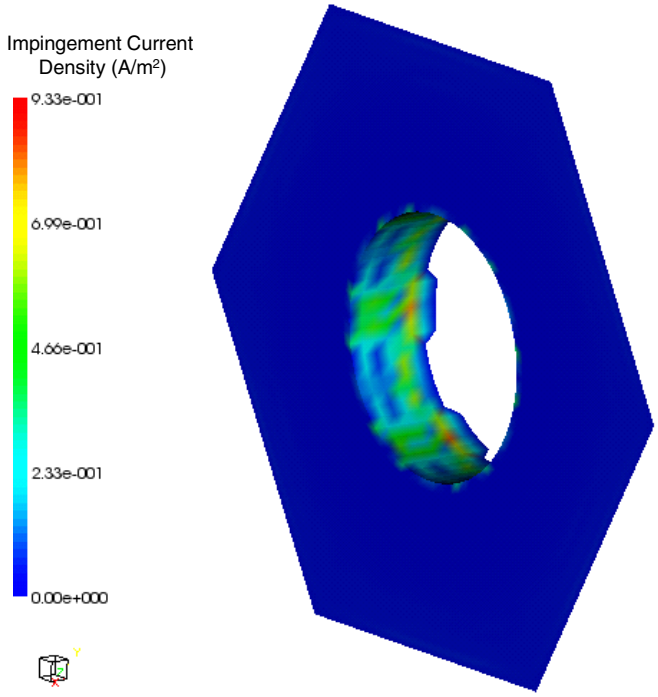

Figure 12. Impingement current on the accelerator grid barrel and downstream face due to crossover impingement for r = 199 mm, J_b = 1.20 A case. Notice that the highest impingement current is deposited in the directions of the hexagon points, which correspond to the webbing direction of the inter-aperture space.

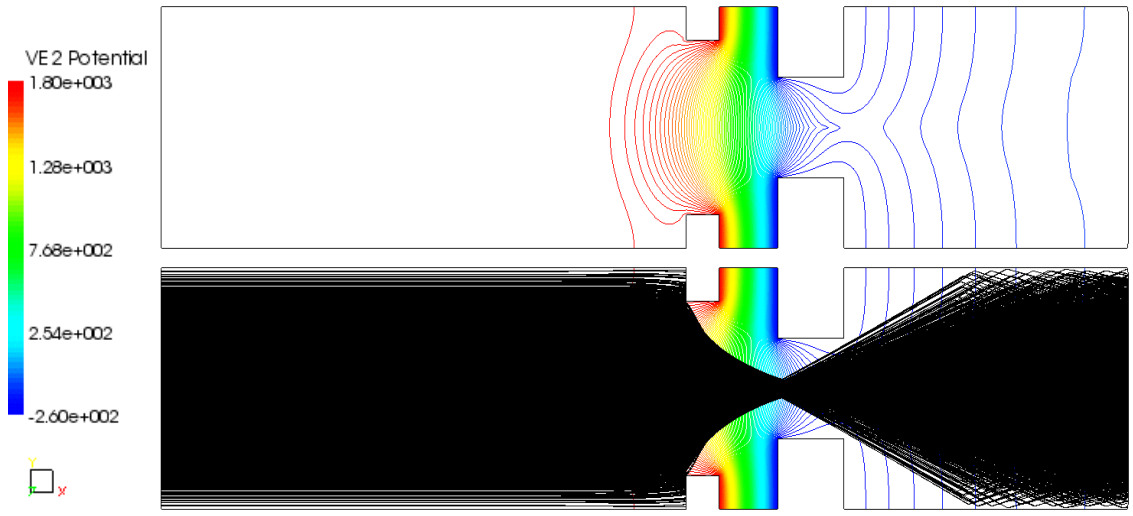

Figure 13. Equipotential lines and particle trajectories for r = 153 mm, J_b = 1.20 A case. Notice that sheath is still established relatively near the screen grid in this case. No crossover impingement is indicated. Boundaries shown are from point to point on the hex boundary condition.

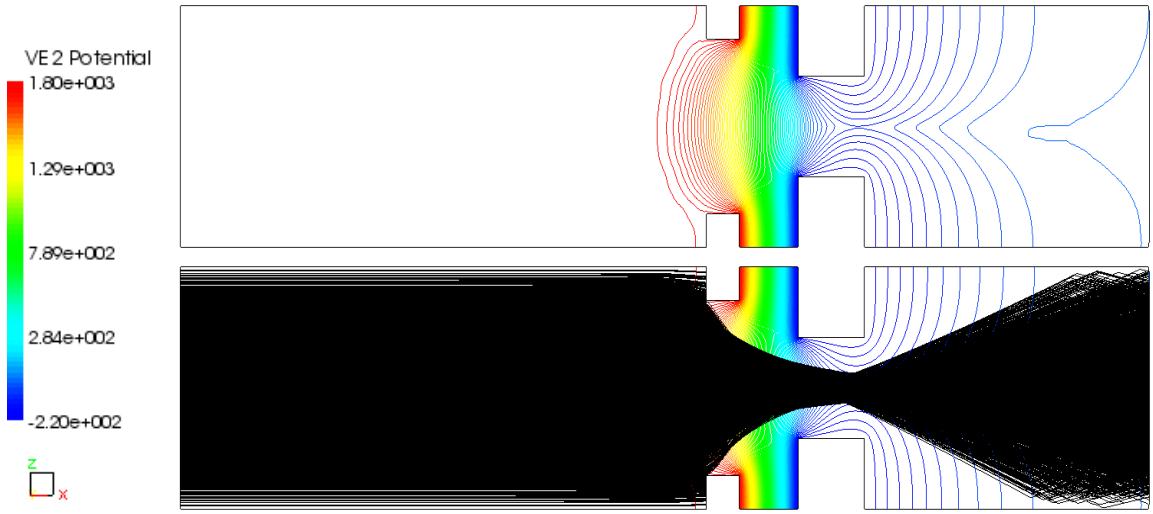

Figure 14. Equipotential lines and particle trajectories for r = 153 mm, J_b = 3.52 A case. The sheath is again established close to the screen grid. No crossover impingement is indicated. The apparent asymmetry in the ion trajectories is most likely due to insufficient run cycles, and not an actual physical effect. Boundaries shown are from point to point on the hex boundary condition.

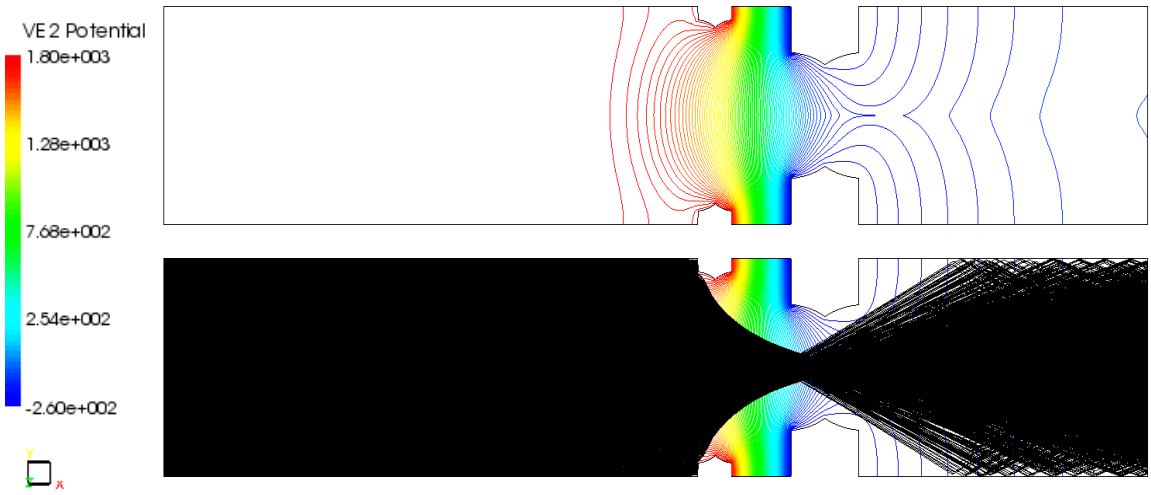

Figure 15. Equipotential lines and particle trajectories for r = 153 mm, J_b = 1.20 A, cusp geometry case. The cusps distort the equipotential lines inside the aperture barrels, but no crossover impingement is indicated. The boundary condition is cylindrical (axisymmetric).

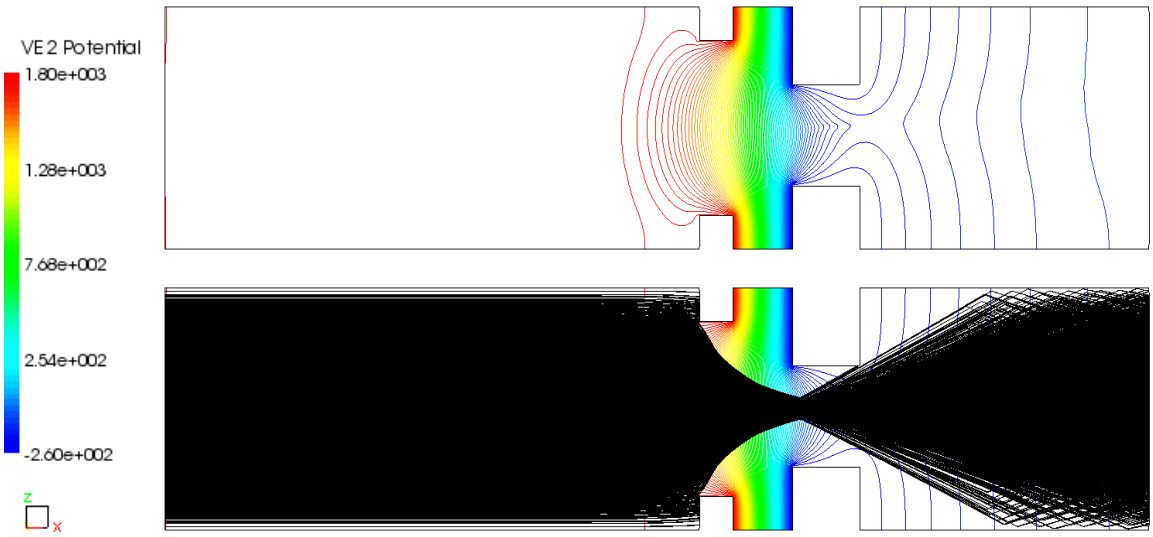

Figure 16. Equipotential lines and particle trajectories for r = 153 mm, J_b = 1.20 A, misaligned aperture case. The sheath is still distorted upstream of the screen grid, and crossover impingement is clearly indicated on the side of the aperture barrel opposite of the misalignment direction. Boundaries shown are from point to point on the hex boundary condition.

REPORT DOCUMENTATION PAGE

Form Approved
OMB No. 0704-0188

1. AGENCY USE ONLY (*Leave blank*)	2. REPORT DATE	3. REPORT TYPE AND DATES COVERED
	August 2004	Technical Memorandum

4. TITLE AND SUBTITLE

Computational Ion Optics Design Evaluations

5. FUNDING NUMBERS

WBS–22–319–20–B2

6. AUTHOR(S)

Shane P. Malone and George C. Soulas

7. PERFORMING ORGANIZATION NAME(S) AND ADDRESS(ES)

National Aeronautics and Space Administration
John H. Glenn Research Center at Lewis Field
Cleveland, Ohio 44135–3191

8. PERFORMING ORGANIZATION REPORT NUMBER

E–14714

9. SPONSORING/MONITORING AGENCY NAME(S) AND ADDRESS(ES)

National Aeronautics and Space Administration
Washington, DC 20546–0001

10. SPONSORING/MONITORING AGENCY REPORT NUMBER

NASA TM—2004-213206
AIAA–2004–3784

11. SUPPLEMENTARY NOTES

Prepared for the 40th Joint Propulsion Conference and Exhibit, cosponsored by AIAA, ASME, SAE, and ASEE, Fort Lauderdale, Florida, July 11–14, 2004. Shane P. Malone and George C. Soulas, NASA Glenn Research Center. Responsible person, Shane P. Malone, organization code 5430, 216–433–9706.

12a. DISTRIBUTION/AVAILABILITY STATEMENT

Unclassified - Unlimited
Subject Category: 20 Distribution: Nonstandard

Available electronically at http://gltrs.grc.nasa.gov

This publication is available from the NASA Center for AeroSpace Information, 301–621–0390.

12b. DISTRIBUTION CODE

13. ABSTRACT ***(Maximum 200 words)***

Ion optics computational models are invaluable tools in the design of ion optics systems. In this study a new computational model developed by an outside vendor for use at the NASA Glenn Research Center (GRC) is presented. This computational model is a gun code that has been modified to model the plasma sheaths both upstream and downstream of the ion optics. The model handles multiple species (e.g. singly and doubly-charged ions) and includes a charge-exchange model to support erosion estimations. The model uses commercially developed solid design and meshing software to allow high flexibility in ion optics geometric configurations. The results from this computational model are applied to the NEXT project to investigate the effects of crossover impingement erosion seen during the 2000-hour wear test.

14. SUBJECT TERMS

Ion thruster; Ion engine; Ion propulsion

15. NUMBER OF PAGES

21

16. PRICE CODE

17. SECURITY CLASSIFICATION OF REPORT	18. SECURITY CLASSIFICATION OF THIS PAGE	19. SECURITY CLASSIFICATION OF ABSTRACT	20. LIMITATION OF ABSTRACT
Unclassified	Unclassified	Unclassified	